Original Article

Establishing an hTERT-driven immortalized umbilical cord-derived mesenchymal stem cell line and its therapeutic application in mice with liver failure

Qi Chen[1,2]*, Meixian Jin[1]*, Simin Wang[1]*, Kexin Wang[3], Liqin Chen[1], Xiaojuan Zhu[4], Ying Zhang[3], Yi Wang[3], Yang Li[3], Shao Li[3], Youmin Zeng[1], Lei Feng[3] iD, Wanren Yang[3], Yi Gao[3] iD, Shuqin Zhou[1] iD and Qing Peng[3] iD

Abstract

Acute liver failure (ALF) is characterized by rapid liver cell destruction. It is a multi-etiological and fulminant complication with a clinical mortality of over 80%. Therapy using mesenchymal stem cells (MSCs) or MSCs-derived exosomes can alleviate acute liver injury, which has been demonstrated in animal experiments and clinical application. However, similar to other stem cells, different cell sources, poor stability, cell senescence and other factors limit the clinical application of MSCs. To achieve mass production and quality control on stem cells and their exosomes, transfecting umbilical cord mesenchymal stem cell (UCMSC) with lentivirus overexpressing human telomerase reverse transcriptase (hTERT) gene, the hTERT-UCMSC was constructed as an immortalized MSC cell line. Compared with the primary UCMSC (P3) and immortalized cell line hTERT-UCMSC at early passage (P10), the hTERT-UCMSC retained the key morphological and physiological characteristics of UCMSC at the 35th passage (P35), and showed no signs of carcinogenicity and toxic effect in mice. There was no difference in either exosome production or characteristics of exosomes among cultures from P3 primary cells, P10 and P35 immortalized hTERT-UCMSCs. Inoculation of either hTERT-UCMSC (P35) or its exosomes improved the survival rate and liver function of ALF mice induced by thioacetamide (TAA). Our findings suggest that this immortalized cell line can maintain its characteristics in long-term culture. Inoculation of hTERT-UCMSC and its exosomes could potentially be used in clinics for the treatment of liver failure in the future.

[1]Department of Anesthesiology, Zhujiang Hospital, Southern Medical University, Guangzhou, Guangdong, China
[2]Department of Anesthesiology, The First Affiliated Hospital of Jinan University, Guangzhou, Guangdong, China
[3]General Surgery Center, Department of Hepatobiliary Surgery II, Guangdong Provincial Research Center for Artificial Organ and Tissue Engineering, Guangzhou Clinical Research and Transformation Center for Artificial Liver, Institute of Regenerative Medicine, Zhujiang Hospital, Southern Medical University, Guangzhou, Guangdong, China
[4]Department of Anesthesiology, The First People' s Hospital of Kashi, Kashgar, Xinjiang, China

*These authors contributed equally to this work.

Corresponding authors:
Shuqin Zhou, Department of Anesthesiology, Zhujiang Hospital, Southern Medical University, No. 253 Industrial Avenue Center, Guangzhou, Guangdong 510515, China.
Email: zhoushuqin@smu.edu.cn

Qing Peng, General Surgery Center, Department of Hepatobiliary Surgery II, Guangdong Provincial Research Center for Artificial Organ and Tissue Engineering, Guangzhou Clinical Research and Transformation Center for Artificial Liver, Institute of Regenerative Medicine, Zhujiang Hospital, Southern Medical University, No. 253 Industrial Avenue Center, Guangzhou, Guangdong 510515, China.
Email: zhujiangzhuanhua@163.com

Graphical abstract
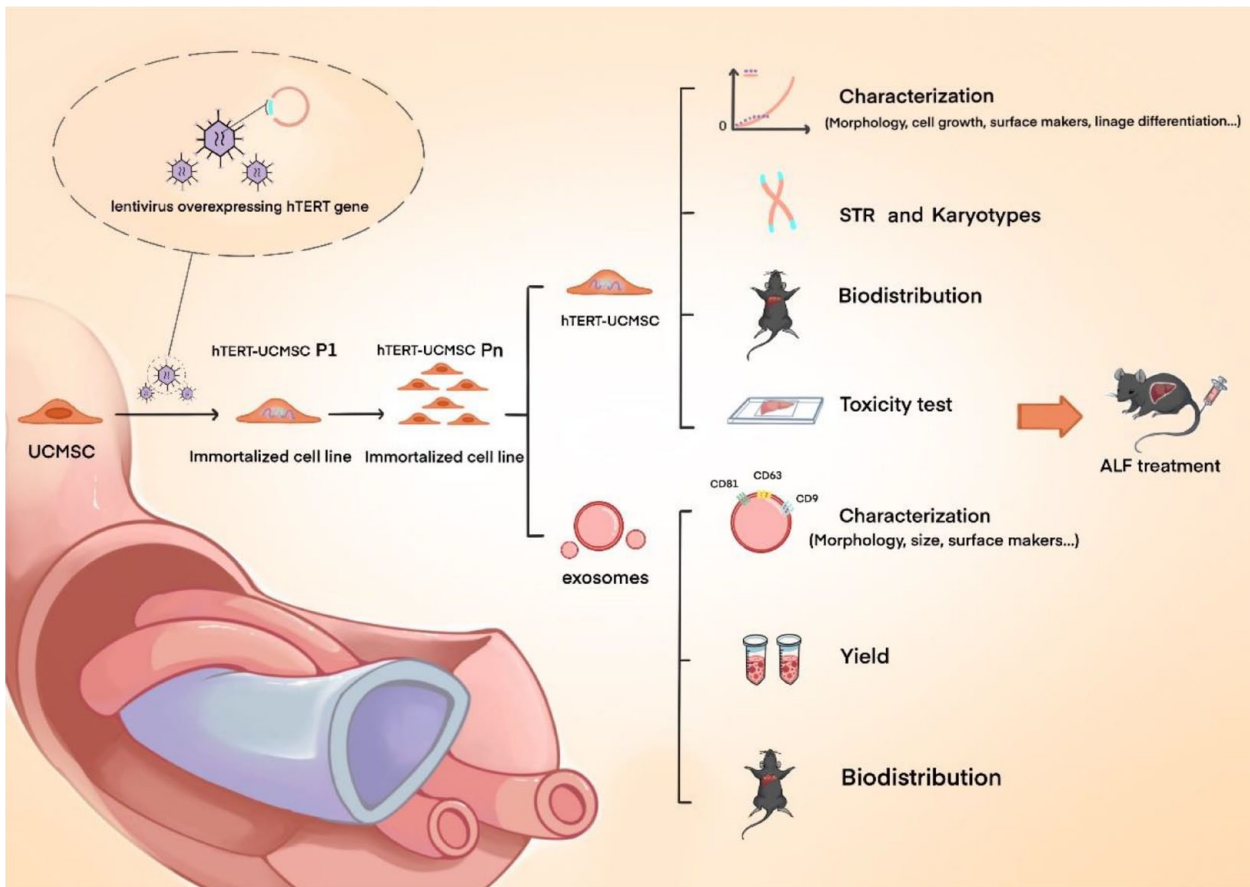
Introduction

Acute liver failure (ALF) is a fatal syndrome characterized by acute deterioration of liver function, extensive necrosis of liver cells, and subsequent multiple organ failure, with a mortality rate of over 80%.[1] ALF is frequently encountered in intensive care units and can be caused by a variety of factors, such as drug toxicity, hepatitis virus infection, and autoimmune hepatitis et al.[2] At present, although a variety of therapeutic strategies have been proposed for ALF treatment, liver transplantation is the most common and effective method. However, due to the limitations of donor organ, high cost, and the need for lifelong immunosuppressive therapy, only a few ALF patients can be treated successfully.[3] Currently, the mortality rate of ALF remains high, posing a serious threat to human health, and an alternative strategy is urgently needed to effectively treat these patients.

For many years, safe and effective interventions for the treatment of end-stage liver failure have been explored.[4] Stem cell therapy has been extensively studied in the field of liver disease. Mesenchymal stem cells (MSCs) play important roles in cell growth and tissue repair. They have anti-apoptosis, angiogenesis, and immunosuppression effects, and have been shown to stimulate liver cell proliferation, regulate inflammatory response, and maintain liver cell

functions.[5,6] Umbilical cord mesenchymal stem cells (UCMSCs) have a number of advantages including low immunogenicity, no tumorigenic effect, easy isolation, and no ethical problems, making it a viable candidate for cell therapy.[7] UCMSCs transplantation therapy has been proved to be one of the promising therapies for ALF in animal models.[8] Paracrine function is an important mechanism of stem cell therapy, and exosomes are important paracrine substances of MSCs.[9] Exosomes mediate cell microcommunication by delivering mRNAs, non-coding RNAs, and proteins between cells,[10,11] and possess the effect of parental MSCs. Exosomes-based therapy have their own advantages as it is safer, easier to transport and administer. Therefore, exosome-based cell-free therapy has potential clinical application prospects. Several studies have demonstrated that inoculation of exosomes produced from UCMSCs is an effective way in treating ALF.[12] Despite the fact that UCMSCs (including their exosomes) have many benefits, their therapeutic applications in clinic face numerous challenges. One of the most difficult challenges is obtaining a scalable UCMSCs with good and stable quality for pharmaceutical manufacturing, as cell senescence and the loss of stem-like potency occurs during sub-culturing, most likely due to telomere shortening.[13] It was reported that long-term in vitro passage of UCMSCs attenuated the therapeutic

effects on acute liver failure in rat.[14] Furthermore, UCMSCs generated from different individual are heterogeneous, which leads to batch-to-batch variation of cells and exosomes and limit their clinical usages.

Immortalized MSCs have been considered to be an alternative to primary mesenchymal stem cells as it can overcome the drawback of cellular senescence and the loss of stem-like property of MSCs. Immortalized MSCs could be a highly expansible supply for mass production of MSCs and their exosomes as therapeutic agents. Previous studies have reported that the ectopic expression of the human telomerase reverse transcriptase (hTERT) gene has been widely used for cell immortalization.[15–18] This method has been proved to be able to improve stem cell properties and reduce the spontaneous differentiation of bone marrow derived human MSCs.[19] However, it needs to be investigated whether immortalized UCMSCs with ectopic hTERT as well as their exosomes have a safe and stable quality after long-term passage. And more importantly, whether inoculation of immortalized UCMSCs or their exosomes is effective to treat acute liver failure.

In this study, we constructed an immortalized cell line, named hTERT-UCMSC by transfecting exogenous hTERT gene into UCMSCs. Compared with the primary UCMSC (P3) and immortalized cell line hTERT-UCMSC at early passage (P10), the hTERT-UCMSC at the 35th passage (P35) still retained the key morphological and physiological characteristics of UCMSCs, and showed no signs of carcinogenic transformation. The exosomes produced from different passages of hTERT-UCMSCs showed similar particle yield and characteristics. Furthermore, inoculation of either hTERT-UCMSCs at the 35th passage or their exosomes was effective in treating mice with liver failure induced by thioacetamide (TAA). Our findings suggest that the hTERT-UCMSC immortalized cell line and their exosomes have promising clinical use in treating liver failure.

Methods

Culture and expansion of UCMSCs

Written informed consent of the donor (puerpera, ID:4083228, age: 37, fetal sex: female) was obtained for this study. UCMSCs was isolated from Wharton's jelly of human umbilical cord by tissue explants method. The study protocols were reviewed and approved by the Zhujiang Hospital review board and ethics committee of Zhujiang Hospital of Southern Medical University (approval number: 2022-KY-003-01). Routine cell culture conditions: serum-free medium (Haoyang, MSC2020-G) +1% penicillin and 1% streptomycin (37℃, 5%CO_2). Under these conditions, the cells grew adherent. Flow cytometry showed that MSCs showed high expression of CD105, CD90, CD73, and CD44, and low expression of CD34, CD19, CD11b, CD45, and HLA-DR, indicating osteogenic, adipogenic, and neurogenic differentiation abilities. It meets the minimum standards set by the International Society for Cell Therapy (ISCT) in 2006.

Transduction of UCMSC with lentiviral vectors

Target gene (hTERT) fragments were designed and synthesized based on gene sequences retrieved from GenBank and a lentiviral recombinant overexpression plasmid hTERT-GV367 (Ubi-TERT-SV40-EGFP-IRES-puromycin) was synthesize by GeneChem (Shanghai, China) (Supplemental Figure S1). The plasmid was also loaded with puromycin gene and EGFP gene. The lentivirus plasmid was transfected into primary UCMSC (P3) at the multiplicity of infection (MOI) of 100. Cells were selected and maintained with puromycin (1 μg/mL, Beyotime, China) after transfection for 72 h.

Reverse transcription-polymerase chain reaction

Total RNA was extracted using Trizol reagent and reverse transcription was performed using M-MLV reverse transcriptase (SYBR® Green Premix Pro Taq HS qPCR Kit, AG11711), random primers and oligonucleotide primers. The miRNA isolated from exosomes was extracted using Trizol reagent and miRNA reverse-transcription kits were used to obtain cDNA following the manufacturer's instructions (miRNA first stand cDNA synthesis kit, AG11716) and SYBR Green was also used for miRNA's qPCR. The mRNA levels of target genes hTERT, Oct4, Sox4 and Nanog, miRNA level of miRNA-126-3P, miRNA-139-5p, miRNA-146a-5p, and miRNA-223-5p were detected by real-time quantitative PCR (RT-PCR). Polymerase chain reactions (PCR) were carried out in a PCR thermal cycler. GAPDH and U6 were used as housekeeping genes to normalize the expression of mRNA and miRNA. Relative RNA levels were calculated using the $2^{-\Delta\Delta CT}$ method. Primer sequences were listed in Table 1.

Western blot

Cells were collected at the designated time points, treated with SDS lysis buffer (Beyotime), and subjected to centrifugation at 10,000*g* at 4℃. Protein separation was achieved using 10% polyacrylamide gels and transferred onto 0.45 μm PVDF membranes (Merck Millipore). The loading quantity of sample of SDS-PAGE was 15 μg total protein. The membrane was blocked with 5% BSA for 1.5 h. The initial and subsequent incubations were conducted following the specified procedural steps. Protein expression was quantified by measuring the intensity of the gray value. The primary antibodies used in this study were TERT (27586-1-AP, Proteintech) and GAPDH (2118, Cell Signaling Technology).

Table 1. Gene primer sequences.

Gene	Forward primer (5′–3′)	Reverse primer (5′–3′)
GAPDH	TGTTGCTGTAGCCATATTCATTGT	CCATTCTTCCACCTTTGATGCT
hTERT	CGTGGTTTCTGTGTGGTGTC	TGGAACCCAGAAAGATGGTC
Oct4	GCTCGAGAAGGATGTGGTCC	CGTTGTGCATAGTCGCTGCT
Sox2	TACAGCATGTCCTACTCGCAG	GAGGAAGAGGTAACCACAGGG
Nanog	GCAGAAGGCCTCAGCACCTA	AGGTTCCCAGTCGGGTTCA
miR-126-3P	TATCAGCCAAGAAGGCAGAA	CGAATTCTAGAGCTCGAGGCAGG
miR-139-5P	ACACTCCAGCTGCACGTGTC	CGAATTCTAGAGCTCGAGGCAGG
miR-146a-5p	CCGATGTGTATCCTCAGCTTTG	CGAATTCTAGAGCTCGAGGCAGG
miR-223-5p	GCGCGCGTGTATTTGACAAGCTGAGTT	CGAATTCTAGAGCTCGAGGCAGG

5-Ethynyl-2′-deoxyuridine (EdU) assay

Cells were seeded in 96-well plates at 5×10^3 per well and cultured for 24 h. The cells were fixed and stained with a BeyoClick™ EdU Cell Proliferation Kit with Alexa Fluor 594 (Beyotime, China) in accordance with the instructions. The number of EdU positive cells was observed by fluorescence microscope. The percentage of EdU positive cells was calculated as the number of EdU-positive cells/ the number of Hoechst-positive cells.

Cell growth curves

2×10^4 cells were cultured in 25 cm² cell culture flask (37℃, 5% CO_2). The fluid was changed twice a week and the cells were sub-cultured every 7 days. The cells were counted using a blood cell counting apparatus. The formula PDL (Population Doubling Level) = (log (Nn/Nn−1))/ log 2 (n: cell algebra; N: cell number) was used to calculate the Cumulative cell population multiplication (CPDs). The cell proliferation curve was plotted.

β-galactosidase activity assay

Primary UCMSC P3 and P10, and hTERT-UCMSC P10 and P35 were inoculated (2×10^3 cells) into six-well plates. After 7 days, the cells were washed with PBS and fixed with fixation mixture (Senescence β-Galactosidase Staining Kit, Beyotime, C0602) for 15 min. Cells were stained by adding 1 mL of the staining mixture to each well. The cells were incubated at 37℃ without CO_2, and the staining was observed by phase contrast microscope 16 h later. Senescent cells were stained by adding 1 mL of the staining mixture to each well.

Flow cytometry analysis

The primary UCMSC P3 and hTERT-UCMSC P35 were respectively identified by flow cytometry. The cells were digested by trypsin, washed, centrifuged, and re-suspended in PBS at the concentration of 1×10^6 cells/mL. Cells were cultured and stained with antibodies against mesenchymal stem cell markers (CD73-APC, CD90-PE, and CD105-PE), hematopoietic and epithelial cell markers (CD19-APC, CD14-APC, CD34-PE, CD45-V500, and HLA-DR-PE) in darkness at 2℃–8℃ for 30 min. All antibodies were purchased from Abcam (Cambridge, UK). After 30 min, the cell suspension was washed twice and suspended in 200 μL PBS again. Flow cytometry was performed and analyzed using a FLOWJ software.

Lipogenic, osteogenic chondrogenic, and neurogenic differentiation potential of hTERT-UCMSC

Primary UCMSC P3 and hTERT-UCMSC P10 and P35 were inoculated into six-well plates with 3×10^4 cells/ well. When the cells reached 80-90% confluence, the serum-free media were removed and lipogenic (Stemcell Technologies), osteogenic (Stemcell Technologies) and neurogenic (Promocell GmbH) induction media were added. The medium in the culture plate for adipogenesis and osteogenic differentiation was changed every 3 days for 15–20 days. The medium in the neurogenic differentiation culture plate was changed every 2 days for 5–7 days. When lipid droplets appeared in the cytoplasm of the adipogenesis induced group, the medium was carefully removed. Then the cells were washed with PBS twice, fixed with 40 g/L paraformaldehyde for 20 min, and stained with oil red O. In the osteogenic induction group, round calcified nodules were observed and cells were stained with alizarin red. On the first day of neurogenic differentiation, significant morphological changes were observed, and Nissl staining was performed at least 5 days after culture.

To induce chondrogenic differentiation of cells (Biological Industries), cells were seeded 1×10^5 cells/ well in 96-well U-bottom culture plate using 100 μL of MSC NutriStem® XF. After 24 h of culture, the medium was changed to complete MSCgo™ Chondrogenic XF medium and cells continued to be cultured for 21 days. The Alcian blue stain (Phygene) was then used to identify chondrogenic differentiation.

Tube formation assay

Primary UCMSC P3 and hTERT-UCMSC P10 and P35 were seeded into $25\,cm^2$ cell culture flask and allowed to reach 60% to 70% confluence. The medium was then changed to serum-free medium (5 mL), and the cells were cultured for another 24 h. Next, the conditioned medium was collected and centrifuged to remove the debris. The conditioned medium was then filtered and stored at −80℃.

Growth Factor Reduced Matrigel (BD Biosciences, 356231) was plated in 96-well plates and incubated at 37℃ for 30 min. Then, human umbilical vein endothelial cells (HUVECs) were re-suspended in the conditioned medium, and HUVECs (2×10^4 cells/well) were seeded on polymerized Matrigel. After incubation at 37℃ for 4 h, tube formation was recorded with an inverted microscope. The total branching points and total tube length were measured using Image J software.

PI/Hoechst 33342 staining

Cells were plated at 6000 cells/well in $100\,\mu L$ of culture medium in 96-well plates. Subsequently, the cells were cultured at 4℃ for 1 and 3 days, respectively. PI (propidium iodide, C2015, Beyotime) was used to label deceased cells while Hoechst 33342 (C1027, Beyotime) to used to label cell nuclei. The cells were then observed under a fluorescence microscope.

Intracellular reactive oxygen species (ROS) determination

Primary UCMSC P3 and hTERT-UCMSC P10 and P35 were plated in 96-well plates and incubated at 37℃ for 12 h, and treated with $0.6\,mM$ H_2O_2 for 6 h. Subsequently, the hydrogen peroxide was removed and incubated with the probe (CA1420, Solarbio) for 30 min. The cells were then observed under a fluorescence microscope.

Cell viability by CCK-8 assay

Cells were plated at 6000 cells/well in 96-well plates in $100\,\mu L$ of culture medium. After the cells were attached, cells were treated with $0.6\,mM$ H_2O_2, respectively. After 6 h, a 1/10 volume of medium from the CCK-8 Test Kit (Japan Tongren Chemical Research Institute) was added to each well in the dark and incubated for 2.5 h. Optical density (OD) was measured with a microplate reader at 450 nm.

Measurement of immunomodulatory factors

The expression levels of immunoregulatory factors such as transforming growth factor-β (TGF-β), interleukin-10 (IL-10) and programmed cell death 1 ligand 1 (PD-L1) in cellular supernatant and exosomes were detected by commercial enzyme-linked immunosorbent assay (DAKEWE, China) kit. The calculated concentration of each cytokine was normalized by the total amount of cells.

Shot tandem repeat test

Short tandem repeats (STR) identification test was performed to confirm the presence of cross contamination of cells. When the number of primary UCMSC P3 and hTERT-UCMSC P10 and P35 exceeded 1×10^6, the cells were collected. Genome-wide DNA was extracted with a genome extraction kit (IGEBio). DNA concentration was measured with a Micro ultraviolet visible spectrophotometer (Thermo fisher, NanoDrop 2000C). Then, the multifluorescence system was amplified using STR-20A kit (ABI 9700 PCR System), and capillary electrophoresis and fragment separation were performed using an ABI3730XL genetic analyzer (Applied Biosystems). Finally, genotyping was performed using GeneMapper®ID software (version number: ID-X 1.5).

Karyotyping

Karyotype analysis was performed according to standardized staining procedures. When the number of UCMSC P3 and hTERT-UCMSC P10 and P35 exceeded 1×10^6, colchicine was added at $0.2\,\mu g/mL$ 2 to 4 h before termination of culture, and cells were collected. The cells were then treated with a hypoosmotic solution (0.075 M potassium chloride) and fixed on the slides with 3:1 methanol-glacial acetic acid solution. The cells were stained with Giemsa. Chromosome analysis was performed on more than 10 metaphase cells in each generation.

Soft agar tumorigenicity test of hTERT-UCMSC

About 0.6% soft agar was prepared at the bottom of the six-well plates, and hTERT-UCMSC P10 and P35 were inoculated into the top of soft agar (0.3%) at 1×10^3/well, and incubated for 30 days. Human hepatoma cells, HepG$_2$, were used as a positive control. The formation of colony was observed and imaged using a phase contrast microscope.

In vivo tumorigenicity test of hTERT-UCMSC

All experiments involving mice have been reviewed and approved by the Animal Ethics Committee of Southern Medical University Zhujiang Hospital (Animal ethical code: LAEC-2021-060).

Balb/c-nu mice of specific pathogen-free (SPF) grade, male, 6 weeks old, were divided into hTERT-UCMSC P10 group, hTERT-UCMSC (P35) group and HepG$_2$ group (positive control) with five mice in each group.

2.5×10^7 cells/mL were suspended in PBS, and $200\,\mu L$ cell suspension (5×10^6 cells) was injected subcutaneously into the back of mice. The same number of HepG$_2$ cells were used as a positive control. After administration, nodules, mass formation, skin ulceration at the injection site of nude mice were observed and recorded. After 8 weeks of continuous observation, mice were sacrificed for tumorigenicity analysis.

Toxicity test of hTERT-UCMSC

C57BL/6J mice (male, 4–6 weeks old, 20–25 g in weight, raised in Experimental Animal Center of Zhujiang Hospital) were adapted to standard laboratory conditions (room temperature: 20°C–22°C, 12 h light/dark cycle, free feeding and drinking).

In order to investigate acute and chronic toxicity of the cells, C57BL/6J mice were randomly divided into 3 groups ($n=3$): control group, acute toxicity group (hTERT-UCMSC 3d), and chronic toxicity group (hTERT-UCMSC 13w). HTERT-UCMSC (P35) suspensions (1×10^8 cells/kg) were injected into tail vein of mice. Mice in control group were injected with the same volume of saline. Mice in acute toxicity group and chronic toxicity group were sacrificed 3 days and 13 weeks after cell inoculation respectively. During the above periods, the general condition of each mouse was observed. Mice in chronic toxicity group were weighed every week. Mice in each group were dissected after the observation periods, and the viscera such as liver, lung, heart, kidney, and spleen were collected, fixed in 4% paraformaldehyde and embedded in paraffin. The tissue sections were dewaxed and rehydrated, stained with HE, and routine histological examination was performed.

Immunofluorescence analyses

To assess the retention of hTERT-UCMSC in the liver, immunofluorescence analysis was performed. The tissue samples were fixed using 4% paraformaldehyde for 20 min, permeabilized with 0.3% EGFP Triton X-100 for 20 min, blocked with 5% BSA for 2 h, and then incubated overnight at 4°C with EGF antibody (1:200, 50430-2-AP, Protientech). Nuclei were counterstained with DAPI (Solarbio), and images were captured using fluorescence microscopy.

Preparation, characterization, and morphology of exosomes

Primary UCMSC (P3) and hTERT-UCMSC P10 and P35 were inoculated in culture flasks. The medium was replaced when the cell confluence reached 80%. After 48 h of culture, the culture of each group was centrifuged twice at 1500g for 15 min. The supernatants were then collected. To isolate exosomes from the supernatants, Ultrafiltration and Size Exclusion Chromatography (SEC) were used.[20]

The supernatant was then filtered using a $0.20\,\mu m$ filter (Merck Millipore, USA) to remove remaining cells, debris and extracellular vesicles larger than exosomes. After filtration, the supernatant is transferred to 100 kDa molecular weight cutoff Amicon Ultra centrifugal filter (Merck Millipore, USA) and centrifuged at 2000g, which is to remove soluble factors less than 100 kDa and concentrate the supernatant. Then total filtered exosome fraction was purified using Exosupur column (Echo Biotech, China) following the manufacturers' instructions. Fractions were condensed with an Amicon Ultra centrifugal filter to a final volume of 0.2 mL. The collected exosomes were stored at −80°C for subsequent experiments.

The morphology of exosomes was observed under a transmission electron microscopy (TEM, Hitachi, Japan).

Exosomes particle quantification and phenotyping

The quantity, particle size and surface protein characteristics of exosomes from cultures of primary UCMSC at P3, hTERT-UCMSCs at P10 and P35 were analyzed by single particle interferometric reflectance imaging sensing (SP-IRIS) using the ExoView platform (Nanoview Biosciences, United States). SP-IRIS uses a multiplex microarray chip for the immune-capture of commonly expressed exosome tetraspanin proteins CD9, CD63 and CD81 (ExoView Human Tetraspanin kit, EV-TETRA-C).[21] Samples were pipetted into the silicon chips coated with individual antibody spots against human CD9, CD63, and CD81 as well as mouse IgG as an isotype control. Image and data analysis for each chip was performed with the ExoView R100 reader and the Nano Viewer 2.8.10 acquisition software (NanoView Biosciences).

Biodistribution of exosomes of UCMSC and hTERT-UCMSC in mice

To further assess the biodistribution in vivo, the exosomes were stained with DiR following the manufacturers' instructions. DiR-stained exosomes were injected into the tail vein at $50\,\mu g/100\,\mu L$ per mouse. After exosome injection, the fluorescence signals from the exosomes trapped in the organs were measured using IVIS Spectrum with excitation/emission wavelength at 745 nm/800 nm. At the end of the experiments (14 days), the mice were sacrificed and dissected. Liver, spleen, heart, lungs, and kidneys were imaged immediately. The average radiant efficiency of the area of interest was evaluated by Living Image software.

Treatment of ALF mice with hTERT-UCMSCs and their exosomes

C57BL/6J mice were randomly divided into six groups: groups of control, ALF, UCMSC (P3-P6) treatment, hTERT-UCMSC P35 treatment, exosomes of UCMSC

P3~P6 (UCMSC-Exo) treatment and exosomes of hTERT-UCMSC P35 (hTERT-UCMSC P35-Exo) treatment. Each group consisted of eight mice. To induce acute liver failure, mice in each group (except the control group) were injected intraperitoneally with the hepatotoxic chemical, thioacetamide (TAA; 600 mg/kg) twice with a 24 h interval. The control group was injected with the same volume of PBS. 4 h after TAA injection, mice in groups of UCMSC treatment and hTERT-UCMSC P35 treatment were administered respectively by tail vein injection with UCMSC and hTERT-UCMSC P35 cell suspensions (concentration: 1×10^6/mL, volume: 0.1 mL). Mice in groups of exosomes of UCMSC P3~P6 treatment and exosomes of hTERT-UCMSC P35 treatment were injected with respective exosomes (concentration: 1 mg/mL, volume: 0.1 mL) through tail vein. Control group and ALF group were injected with the same volume of cell-free PBS. Mice were observed for 14 days and weighed every week. The survival time and rate of mice were recorded.

Biochemical assay and histological analysis

In the same way as above, C57BL/6J mice were randomly divided into six groups: control group, ALF group, UCMSC P3~P6 treatment group, hTERT-UCMSC P35 treatment group, exosomes of UCMSC P3~P6 treatment and exosomes of hTERT-UCMSC P35 treatment. On the 3rd day and 13th week after PBS or cell suspension or exosomes inoculation, surviving mice in each group were anesthetized with 1% pentobarbital. The blood was taken from the heart, and serum was separated. Serum alanine aminotransferase (ALT), aspartate aminotransferase (AST), albumin (ALB) and total bilirubin (TBIL) were determined by automatic biochemical analyzer (FUJIFILM). Then, liver tissues were isolated, fixed with 4% paraformaldehyde, and paraffin embedded. The sections were dewaxed and rehydrated, stained with hematoxylin eosin (H&E) for routine histological examination

Statistics

The results are expressed as mean ± standard deviation. The student t test was used for between two-group analyses. One-way analysis of variance (ANOVA) was used to compare data among three or more groups. All analyses were performed using Prism 8 software (GraphPad). $p < 0.05$ was considered statistically significant.

Results

HTERT-UCMSC retained proliferation ability in long-term culture

Our results showed that the primary UCMSCs could not continue cell division indefinitely and showed obvious signs of senescence after 10 generations of culture (CPDs = 22), accompanied by reduced proliferative rate and highly vacuolated cytoplasm (Figure 1(a)).

To establish a stable immortalized cell line derived from human umbilical cord stem cells, hTERT-UCMSC, UCMSCs were transfected with lentivirus overexpressing hTERT gene. Similar to the primary UCMSCs, hTERT-UCMSCs are adherent cells with fibroblast-like morphology arranged in parallel or spiral shape. Successful lentivirus transduction was detected by high-content fluorescence signals of EGFP (Figure 1(b)). RT-PCR results showed that the gene expression level of hTERT in P10 and P35 of hTERT-UCMSC was significantly increased compared to the primary UCMSC (P3), both of which was more than 10 times that of primary UCMSC (P3) ($p < 0.001$, Figure 1(c)). Similarly, hTERT protein expression in P10 and P35 of hTERT-UCMSC was also significantly higher than that of primary UCMSC (P3) ($p < 0.001$, Figure 1(d)).

The EdU assay was conducted to test the ability of cells to proliferate. The results demonstrated that both P10 and P35 of hTERT-UCMSC exhibited a significantly higher ability to proliferate when compared to primary UCMSC (P3 and P10) (Figure 1(a)). As shown in the growth curve, hTERT-UCMSC was cultured under conventional condition (37 °C, 5% CO_2), and before submission of this paper, the proliferation of hTERT-UCMSC had exceeded 50 passages (CPDs > 200), and the cells still retained an active division state. By contrast, primary UCMSC proliferation could only be passed fewer than 10 passages (CPDs = 22) cell senescence occurred (Figure 2(c)). Compared with the original UCMSC, hTERT-UCMSC showed markedly increased proliferation ability. A significant increase in activity of β-galactosidase was detected in primary UCMSC as passage number increased, while no significantly increased β-galactosidase activity was observed in hTERT-UCMSC even after 35 passages (Figure 2(d)). These results indicate that the overexpression of hTERT can enhance cell proliferation and division, and delay cell senescence in long-term culture.

HTERT-UCMSC maintained the main characteristics of primary UCMSC in long-term culture

The results of qPCR showed that the expression of Oct4 (1.000 ± 0.1971 vs 0.2988 ± 0.0769, $p < 0.01$), Sox2 (1.000 ± 0.1042 vs 0.2988 ± 0.0769, $p < 0.01$), and Nanog (1.000 ± 0.0656 vs 0.1660 ± 0.0764, $p < 0.01$) of P10 primary UCMSCs was significantly down-regulated compared with P3 primary UCMSCs, indicating that the expression of these genes decreased as the number of passages increased. In contrast, the expression of Oct4 and Nanog genes in hTERT-UCMSC at both P10 and P35 were significantly higher than those in primary UCMSC P3
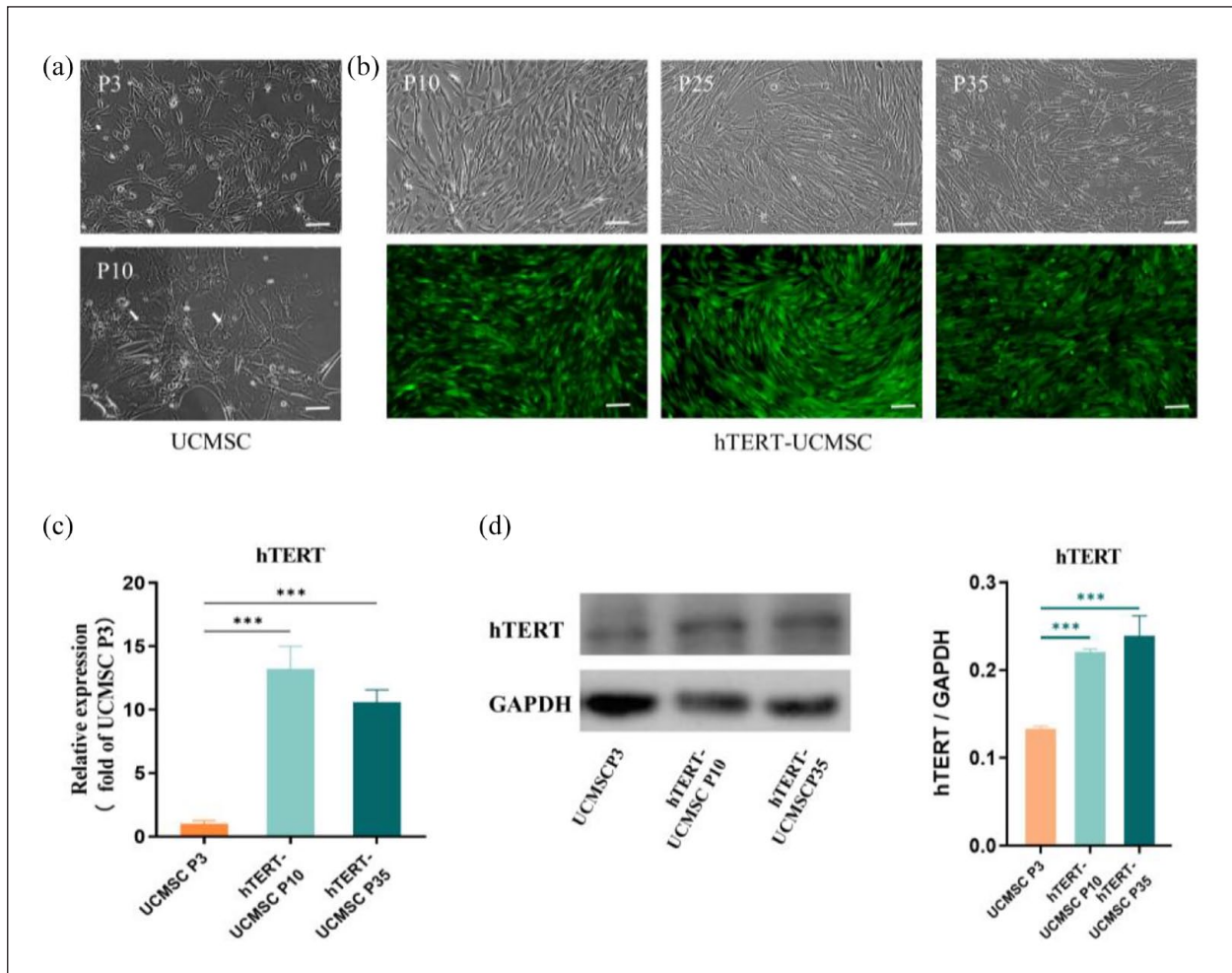
Figure 1. Cell characteristics of UCMSC and hTERT-UCMSC. (a) Morphology of primary UCMSC at passage 3 and passage 10. Arrows indicate cytoplasmic vacuolation. (b) The upper panels represent the morphology of hTERT-UCMSC in different passages under a bright field microscope, and the lower panels represent the morphology of hTERT-UCMSC under a fluorescence microscope. Successful lentivirus transduction was detected by high-content fluorescence microscopy of EGFP signals. (c) The expression of hTERT gene in primary UCMSC and hTERT-UCMSC detected by qPCR analysis. (d) Representative images of Western blot and quantitative analysis of hTERT protein levels. Data are expressed as the mean $\pm$ SEM. $n = 3$. $**p < 0.01$, $***p < 0.001$. Scale bar = 100 μm.

($p < 0.01$). No difference in expression of Oct4 and Nanog was observed between P10 and P35 hTERT-UCMSC. The expression level of Sox2 of hTERT-UCMSC at P10 and P35 was similar to that of UCMSC P3 (Figure 3(a)). These data demonstrate that overexpression of hTERT enhanced the expression of stemness-associated genes in UCMSCs.

Flow cytometry analysis showed that primary UCMSCs (P3) expressed specific cell surface markers of MSCs, including CD73 (99.77%), CD90 (99.83%), and CDl05 (98.94%). UCMSCs had low expression of hematopoietic and epithelial cell specific markers CD19, CD14, CD34, CD45, and HLA-DR (Figure 3(b)). HTERT-UCMSC at the thirty-fifth passage showed high expression of CD73 (100%), CD90 (98.86%), and CDl05 (73.58%), and low expression of CD19, CD14, CD34, CD45, and HLA-DR (Figure 3(c)). These results indicate that there are no apparent changes in expression of specific markers between primary UCMSC and long-term cultured hTERT-UCMSC.

The multilineage differentiation potential of cells was measured by culturing the cells under defined differentiation conditions. HTERT-UCMSC showed similar differentiation capacity to the primary UCMSC. Like UCMSC P3, both hTERT-UCMSC P10 and P35 could be induced to differentiate into adipogenic, osteogenic, chondrogenic, and neurogenic cell lineages, as revealed by positive staining for Oil Red O, Alizarin Red, Alcian Blue, and Nissl staining, respectively (Figure 3(d)).
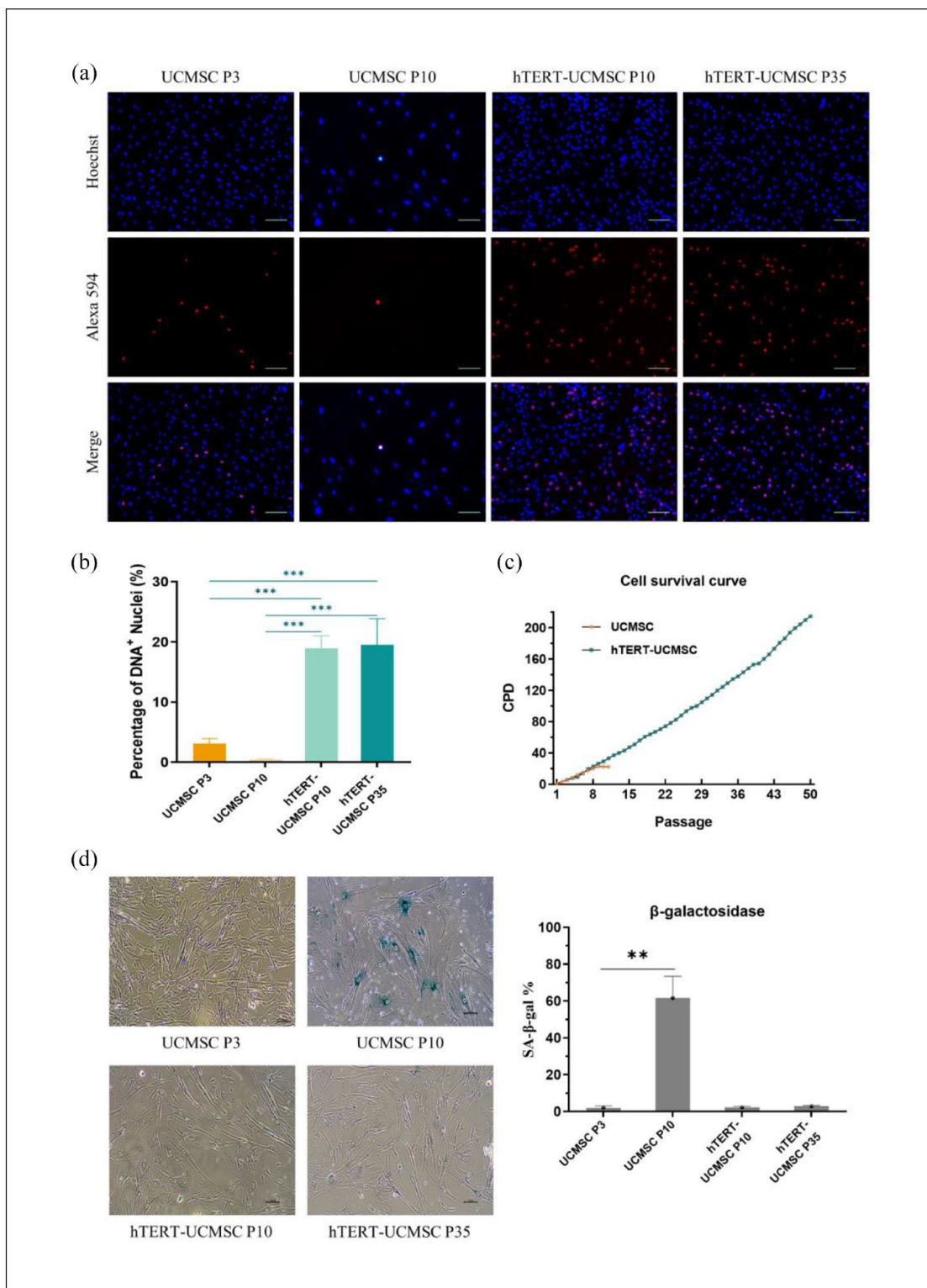
Figure 2. Cell proliferation capacity of UCMSC and hTERT-UCMSC. (a) EdU staining of primary UCMSC and hTERT-UCMSC, Blue (Hochest), Red (Alexa 594). (b) Quantitative analysis of the percentages of EdU-positive cells. (c) The cell growth curve of primary UCMSC and hTERT-UCMSC. (d) Left shows representative images of SA-β-Gal-positive cells, and right shows percentage of SA-β-Gal positive cells in different passages of UCMSC and hTERT-UCMSC. UCMSC P3 is used as the control group. Data are expressed as the mean ± SEM. $n = 3$. ***$p < 0.001$. Scale bar = 100 μm.
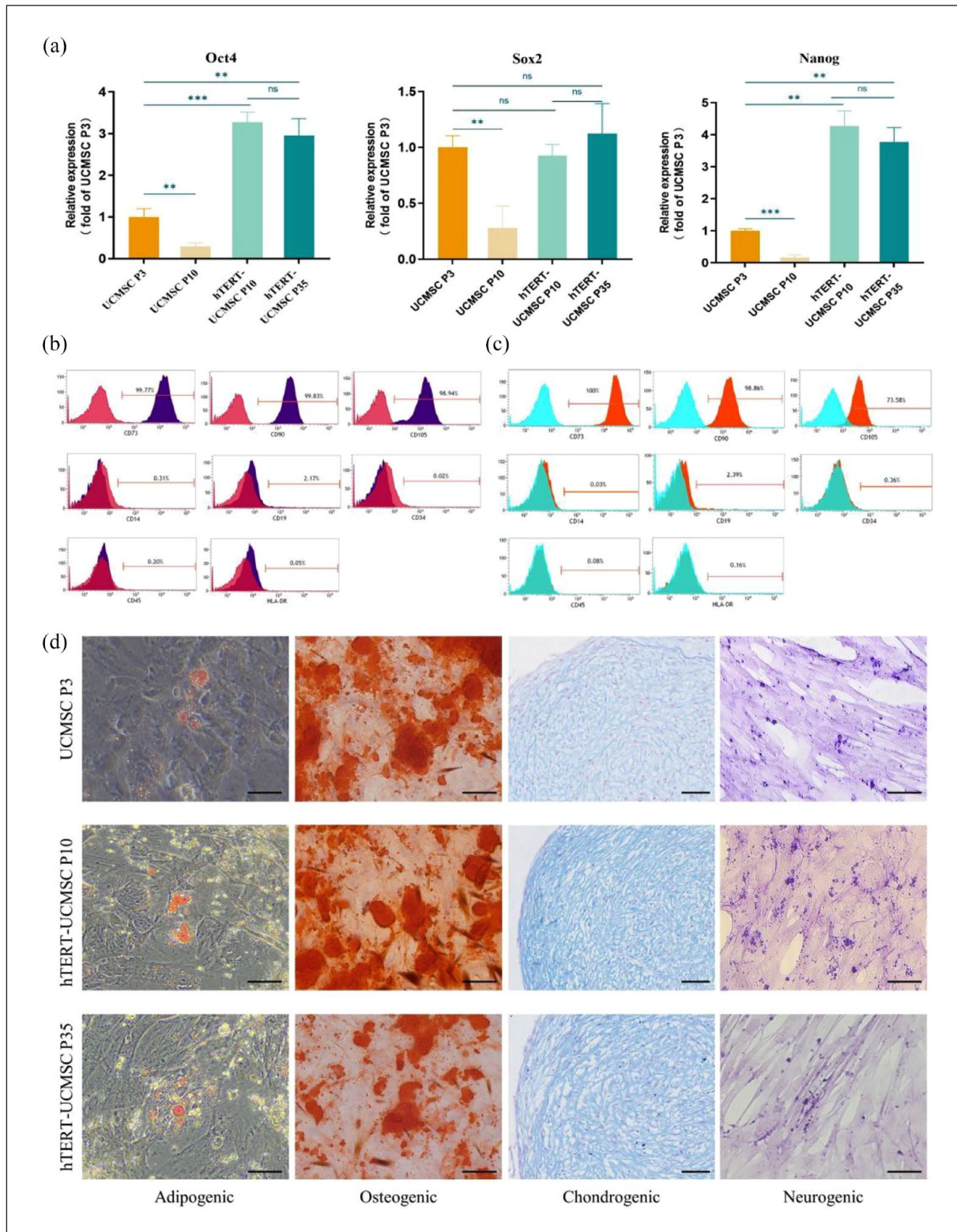
Figure 3. The main characteristics of cells. (a) RT-PCR analysis of the expression of Oct-4, Sox2, and Nanog in hTERT-UCMSC. UCMSC P3 is used as the control group. Cell surface marker of UCMSC P3 (b) and hTERT-UCMSC P35 (c) as assessed by flow cytometry. (d) UCMSC P3 and hTERT-UCMSC P10 and P35 were induced to differentiate for adipogenesis, osteogenesis, chondrogenesis, and neurogenesis. Data are expressed as the mean $\pm$ SEM. $n = 3$. $*p < 0.05$, $**p < 0.01$, $***p < 0.001$. Scale bar $= 100\,\mu m$.

HTERT-UCMSC has the potential to promote angiogenesis

The pro-angiogenic potential of the conditioned medium from UCMSC and hTERT-UCMSC was assessed using a tube forming assay. The data revealed a significant decrease in the ability of senescent UCMSC (P10) to promote HUVEC tube formation (Supplemental Figure S2A). Conversely, immortalized UCMSC (P10 and P35) displayed a comparable ability to promote the formation of an endothelial network as primary UCMSC P3 (Supplemental Figure S2A).

HTERT-UCMSC exhibits a superior stress tolerance than primary UCMSC

UCMSC (P3) and hTERT-UCMSC (P10 and P35) were subjected to low temperature treatment (4℃) to assess their resistance to cryogenic damage. The results indicate that UCMSC exhibited a significantly higher cell mortality rate compared to hTERT-UCMSC at P10 and P35 on day 1 and day 3 (Supplemental Figure S2B). Additionally, after exposure to 0.6 mM H2O2 for 6 h, UCMSC P3 displayed a significantly higher level of reactive oxygen species (ROS) compared to hTERT-UCMSC P10 and P35 ($p < 0.001$, Supplemental Figure S2C, D). At the same time, the cell viability measured by CCK-8 assay showed that the cell viability of UCMSC P3 was significantly lower than that of the other two groups ($p < 0.001$, Supplemental Figure S2E). These results suggest that hTERT-UCMSC exhibits a superior stress tolerance than primary UCMSC.

HTERT-UCMSCs showed good immunomodulatory properties

To assess the ability of cells to secrete immunomodulators, we analyzed the expression of TGF-β, IL-10, and PD-L1 in different passages of cells using an ELISA kit. Compared with the primary UCMSC, the secretion capacity of the above inflammatory regulators in the immortalized cells (P10 and P35) were maintained at a relatively stable level (Figure 4(a)). There was no statistically significant difference among the three groups of cells ($p > 0.05$).

HTERT-UCMSC was an uncontaminated cell line

Short tandem repeat (STR) loci are composed of short linked repeats of 3–7 base pairs in length, which can be used as highly polymorphic markers and can be detected by PCR. Alleles at STR gene seats can be distinguished by the copy number of repeats in the amplification region, and cross-contamination can be determined by comparing the obtained STR typing results with the professional cell STR database. Through the analysis of the cells of primary UCMSC and different generations of hTERT-UCMSC (P10 and P35), no locus more than two allelic peaks were found at any of the 21 loci tested, indicating that hTERT-UCMSC is an uncontaminated cell line (Figure 4(b)).

HTERT-UCMSCs maintained normal karyotype in long-term culture

According to karyotype analysis, the primary UCMSC had a diploid chromosome number of $2n = 46$, consisting of 22 pairs of autosomes and a pair of sex chromosomes. Similar results were found in hTERT-UCMSC P10 and P35 (Figure 4(c)). It could be seen that normal diploid chromosomes were preserved in hTERT-UCMSC after long-term passages.

HTERT-UCMSCs had no tumorigenicity in vivo and in vitro

Soft agar allows cell colonies to grow in three dimensions. To evaluate the tumorigenicity of hTERT-UCMSC in vitro, HepG2 (positive control) and hTERT-UCMSC P10 and P35 were inoculated into soft agar. A large number of colonies were observed in HepG2 group after 30 days. No colonies were observed in the hTERT-UCMSC group (Figure 5(a)).

To evaluate the tumorigenesis of hTERT-UCMSC in vivo, HepG2 (positive control), hTERT-UCMSC P10 and P35 were injected subcutaneously into the back of BALB/c-nu mice. No tumor formation was observed in mice ($n = 5$) injected with hTERT-UCMSC during an 8-week period. In contrast, obvious tumor tissue was formed subcutaneously in mice injected with HepG2 within 8 weeks, and tumor nests were observed by HE staining after sectioning (Figure 5(b)).

HTERT-UCMSCs showed no acute or chronic toxicity

After 13 weeks of cell inoculation, the mice grew well without abnormal appearance or death. The mice in acute toxicity group and chronic toxicity group were dissected respectively at 3 and 13 weeks after inoculation with hTERT-UCMSC P35. Main organs (heart, liver, spleen, lung, and kidney) were harvested for histopathological analysis. There is no difference in the body weight of mice in chronic toxicity group compared to the mice in control group. No obvious abnormalities were observed in the morphology, size, texture and color of each organ, and no tumor was formed. The results of HE staining of organs showed no obvious tissue abnormalities either on the 3rd day on 13th day after cell inoculation (Figure 5(c)).

The hTERT-UCMSC (P35) cells were intravenously administered to mice via the tail vein. The distribution of cells in the liver could be tracked by observing the fluorescence signal of EGFP. Subsequent immunofluorescence
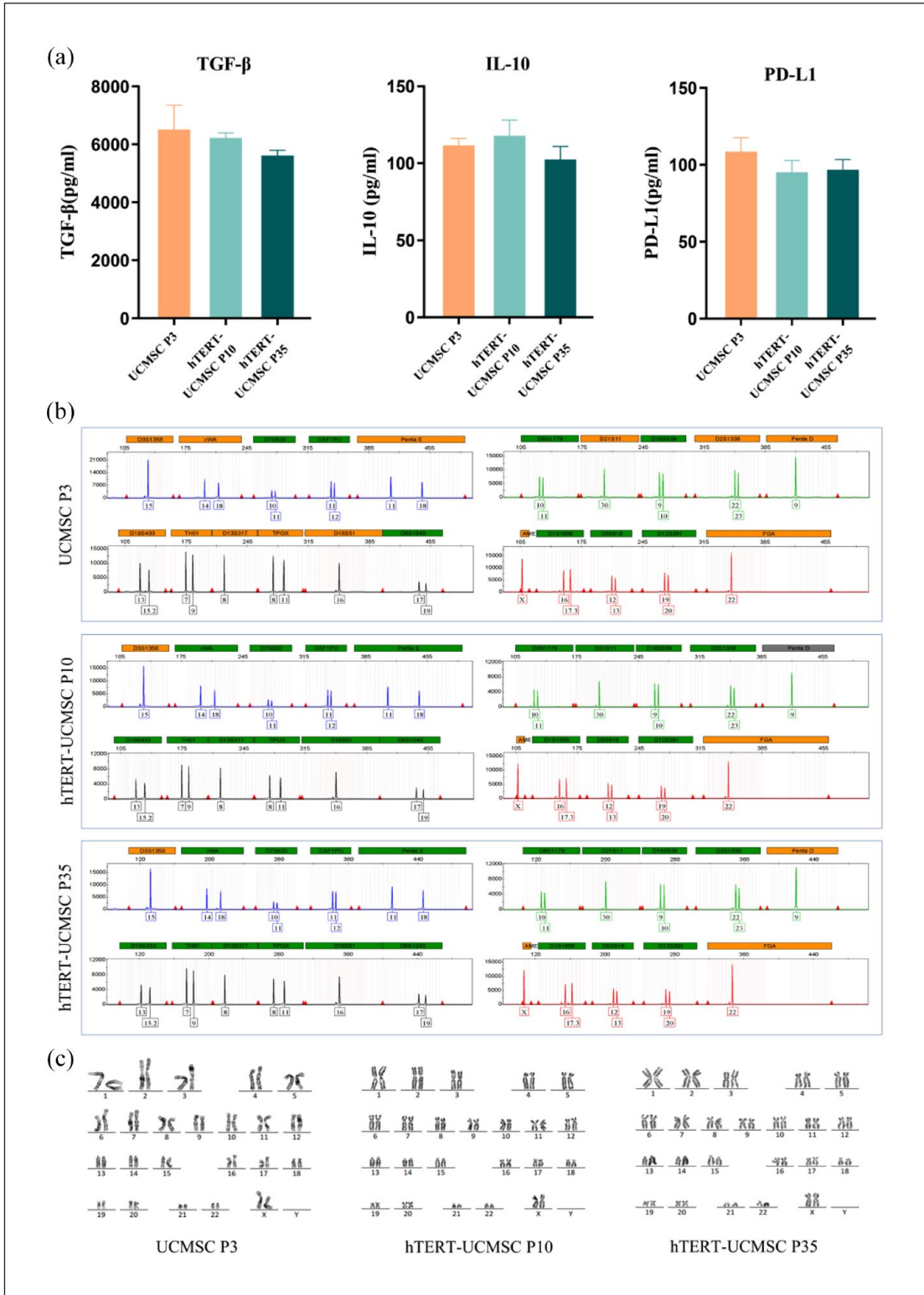
Figure 4. Analysis on STR pattern, karyotype and the expression of inflammatory mediators in different cells. (a) ELISA was used to detect the expression of immunomodulators, TGF-β, IL-10, and PD-L1 ($n = 3$). (b) STR analysis of primary UCMSC P3 and hTERT-UCMSC (P10 and P35). There was no cross-contamination of hTERT-UCMSC in different passages of cells. (c) All karyotypes of UCMSC P3 (primary), hTERT-UCMSC P10 and P35 are 46 XX.
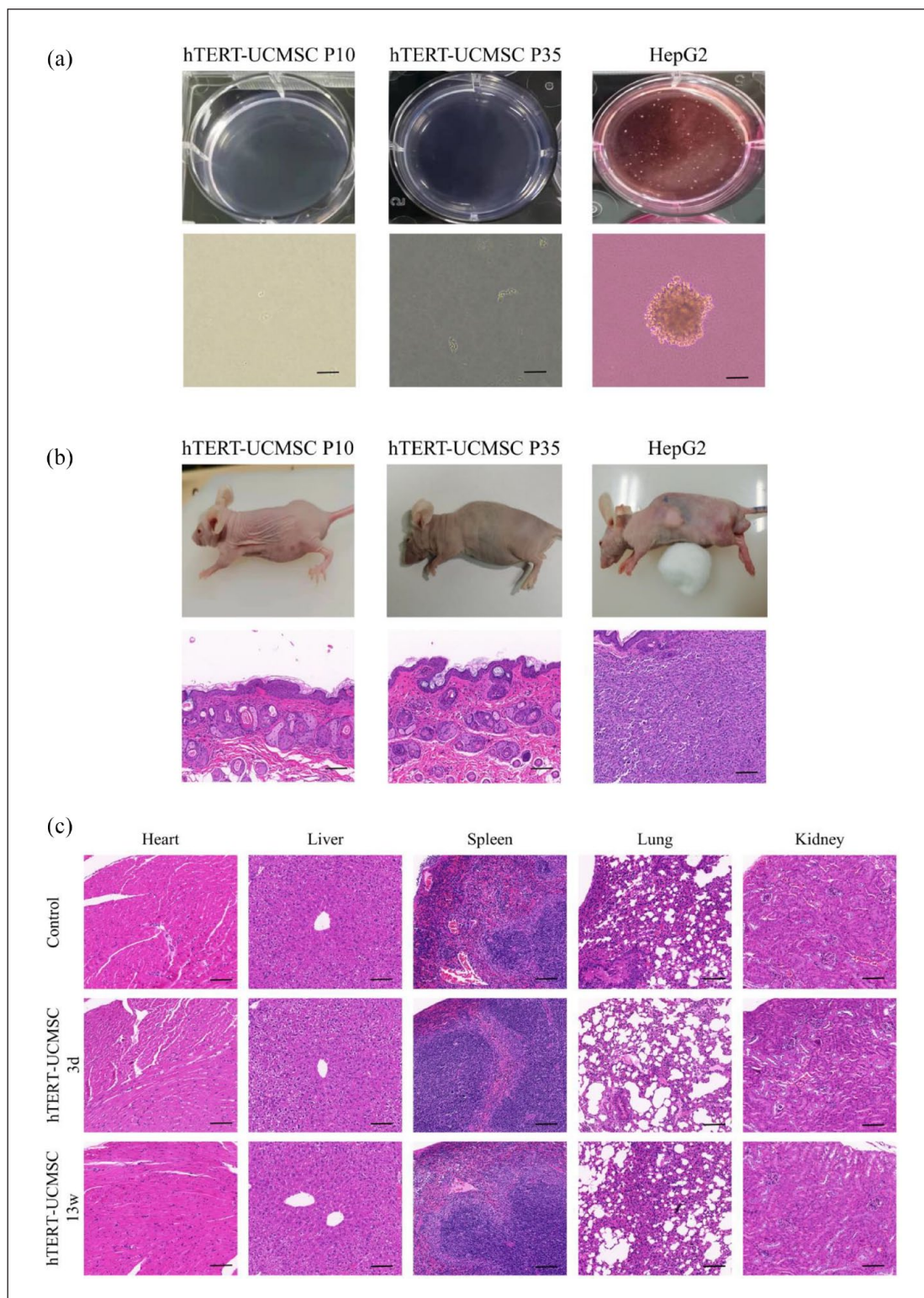
Figure 5. Safety evaluation: (a) soft agar tumorigenicity test, (b) in vivo tumorigenicity test, and (c) H&E staining of tissues from mice with and without cell inoculation. The scale bar = 100 μm.
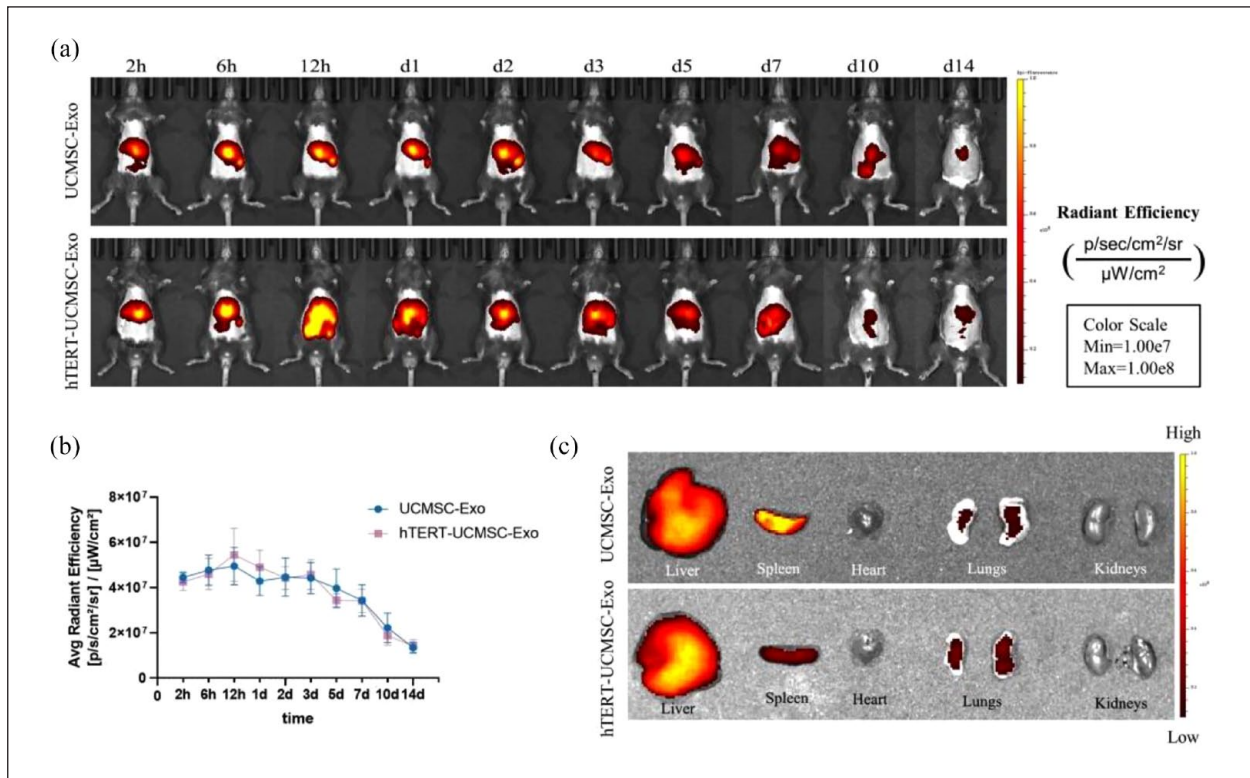
Figure 6. Biodistribution of exosomes of UCMSC and hTERT-UCMSC in mice after intravenous administration: (a) representative images from mice infused with DiR-labeled UCMSC-Exo and hTERT-UCMSC-Exo at different time points, (b) quantification analysis of fluorescence intensity in the region of liver with exosomes infusion ($n = 5$), (c) and representative images of organs from mice infused with DiR-labeled UCMSC-Exo and hTERT-UCMSC-Exo at day 14.

examination of liver tissue sections revealed a discernible cellular distribution of hTERT-UCMSC at 2 h after cell injection (Supplemental Figure S3). The cellular distribution notably decreased on day 3 after cell injection, and by day 5, the cells were essentially eliminated (Supplemental Figure S3).

Biodistribution of exosomes of UCMSC and hTERT-UCMSC in mice

To detect the distribution of exosomes in mice, the exosomes were labeled with DiR and injected into mice through the tail vein. The fluorescence signals of exosomes were measured by the IVIS Spectrum for 14 days. The fluorescence signals were mainly accumulated in the liver and spleen (Figure 6(a)). The fluorescence signals in the livers could be observed as early as 2 h after exosomes injection. The signals remained at a high level for 1–3 days and peaked at 12 h. The signals began to decrease on the fifth day, and the signals were still detectable on the 14th day after exosomes injection (Figure 6(b)). On day 14, the mice were sacrificed and the major organs (liver, spleen, heart, lungs, and kidneys) were imaged. It could be seen

that fluorescence signals on day 14 were mainly accumulated in the livers and spleens, and some signals observed in the lungs, but no signals were observed in the heart and kidneys (Figure 6(c)).

The exosome extracted from hTERT-UCMSC are similar to those from UCMSC

Exosomes were isolated from the conditioned media of primary UCMSC P3 and hTERT-UCMSC (P10 and P35), and identified based on morphology, particle size, concentration, and surface markers. Transmission electron microscopy revealed that these exosomes had a typical cup-shaped morphology (Figure 7(a)). SP-IRIS analysis indicated that the CD63-positive, CD81-positive, CD9-positive exosomes from hTERT-UCMSC were not significantly increased or decreased compared with those from UCMSC, and the exosome yield of P10 hTERT-UCMSC and P35 hTERT-UCMSC was similar (Figure 7(b)). The SP-IRIS showed similar size (diameters range from 56 to 59 nm) of UCMSC-Exo and hTERT-UCMSC-Exo (Figure 7(c)). Immuno-colocalization imaging indicated that these exosomes expressed the exosomal markers CD9, CD63, and CD81 (Figure 7(d)).
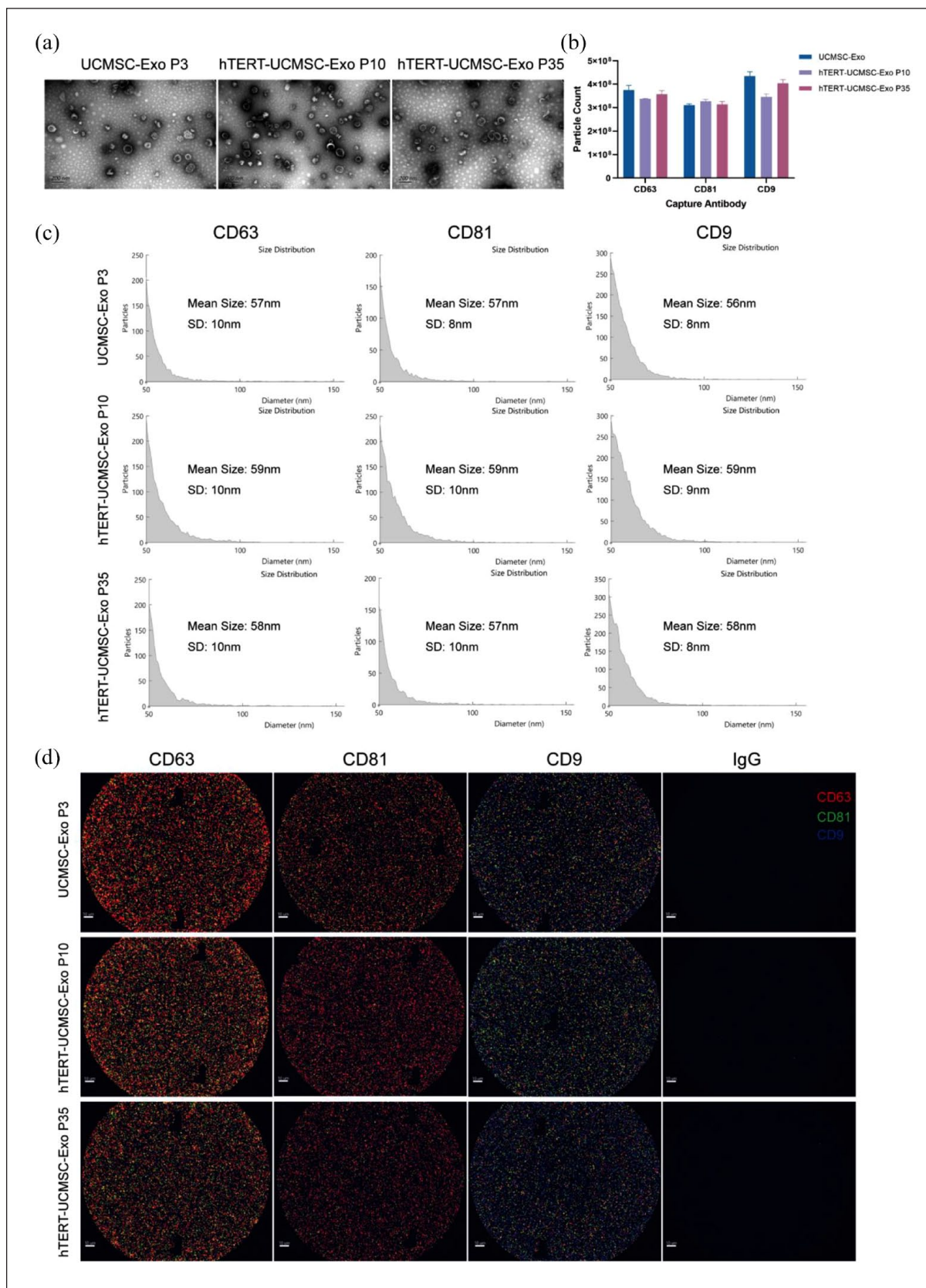
Figure 7. UCMSC and hTERT-UCMSC have the similar exosome production and characteristics: (a) transmission electron microscopy identified the shape of exosomes, scale bar = 200 nm, (b) number of different antibody captured exosomes analyzed by SP-IRIS (*n* = 3), (c) size distribution of exosomes were performed by SP-IRIS, and (d) exosome surface markers (CD9, CD63, CD81) were captured by SP-IRIS. Anti-mouse IgG is the negative control, scale bar = 10 μm.
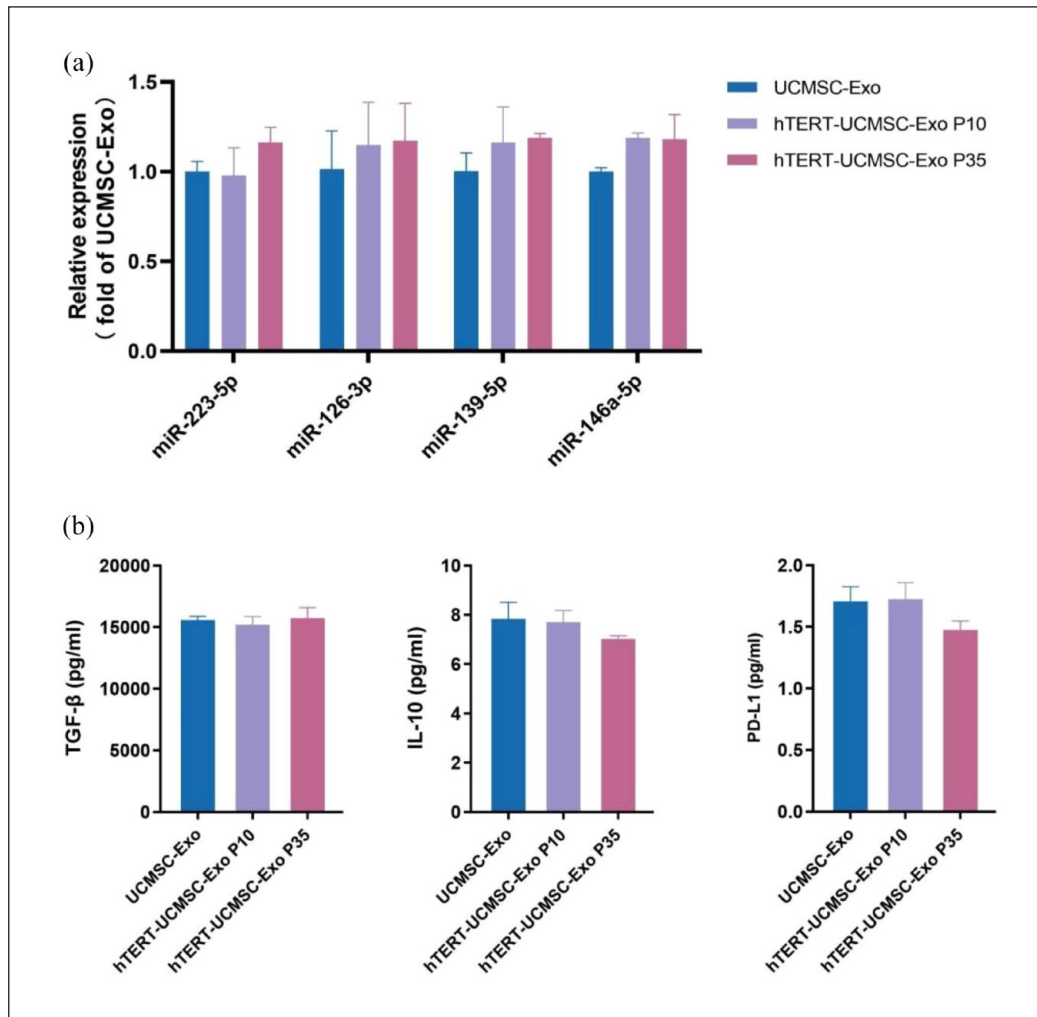
Figure 8. Comparison of components of exosomes derived from UCMSC and hTERT-UCMSC. (a) The expression of miRNA-126-3p, miRNA-139-5p, miRNA-146a-5p, and miRNA-223-5p in exosomes derived from UCMSC and hTERT-UCMSC detected by RT-PCR. (b) The levels of immunomodulators TGF-β, IL-10, and PD-L1 in cell-derived exosomes detected by ELISA ($n=3$).

## Comparison of composition of exosomes derived from UCMSC and hTERT-UCMSC

RT-PCR results showed that the expression levels of miRNA-126-3P, miRNA-139-5p, miRNA-146a-5p, and miRNA-223-5p in hTERT-UCMSC-derived exosomes were similar to those of primary UCMSC (Figure 8(a)). Additionally, ELSA data revealed that hTERT-UCMSC-derived exosomes exhibited no significant change in levels of inflammatory regulators, including TGF-β, IL-10, and PD-L1, when compared to primary UCMSC (Figure 8(b)).

HTERT-UCMSC and hTERT-UCMSC-Exo reduce mortality and alleviate liver injury in TAA-induced mouse models

The effects of inoculation of primary UCMSC (P3~P6), hTERT-UCMSC P35 and their exosomes on TAA-induced

acute liver injury were evaluated. Data were analyzed by Kaplan-Meier method. The observation period was 14 days, and the results showed that the survival rate of the ALF group was 25%, while that of the UCMSC, hTERT-UCMSC P35, and UCMSC-Exo treatment group was 75%. The hTERT-UCMSC-Exo treatment group was 62.5% (Figure 9(b)). Intravenous injection of UCMSC, hTERT-UCMSC P35, UCMSC-Exo, hTERT-UCMSC-Exo significantly increased the survival rate of mice with ALF, and there was no significant difference between the four treatment groups.

To evaluate the therapeutic effects of hTERT-UCMSC and its exosomes on ALF mice, serum ALT, AST, ALB, and TBIL were measured on day 3 after treatment to evaluate the liver function of mice (Figure 9(c)). Compared with the control group, The AST, ALT and TBIL values of TAA treated mice were 8.28 ($p<0.001$), 11.11 ($p<0.001$), and 1.71 ($p<0.01$) times higher than those of control mice,
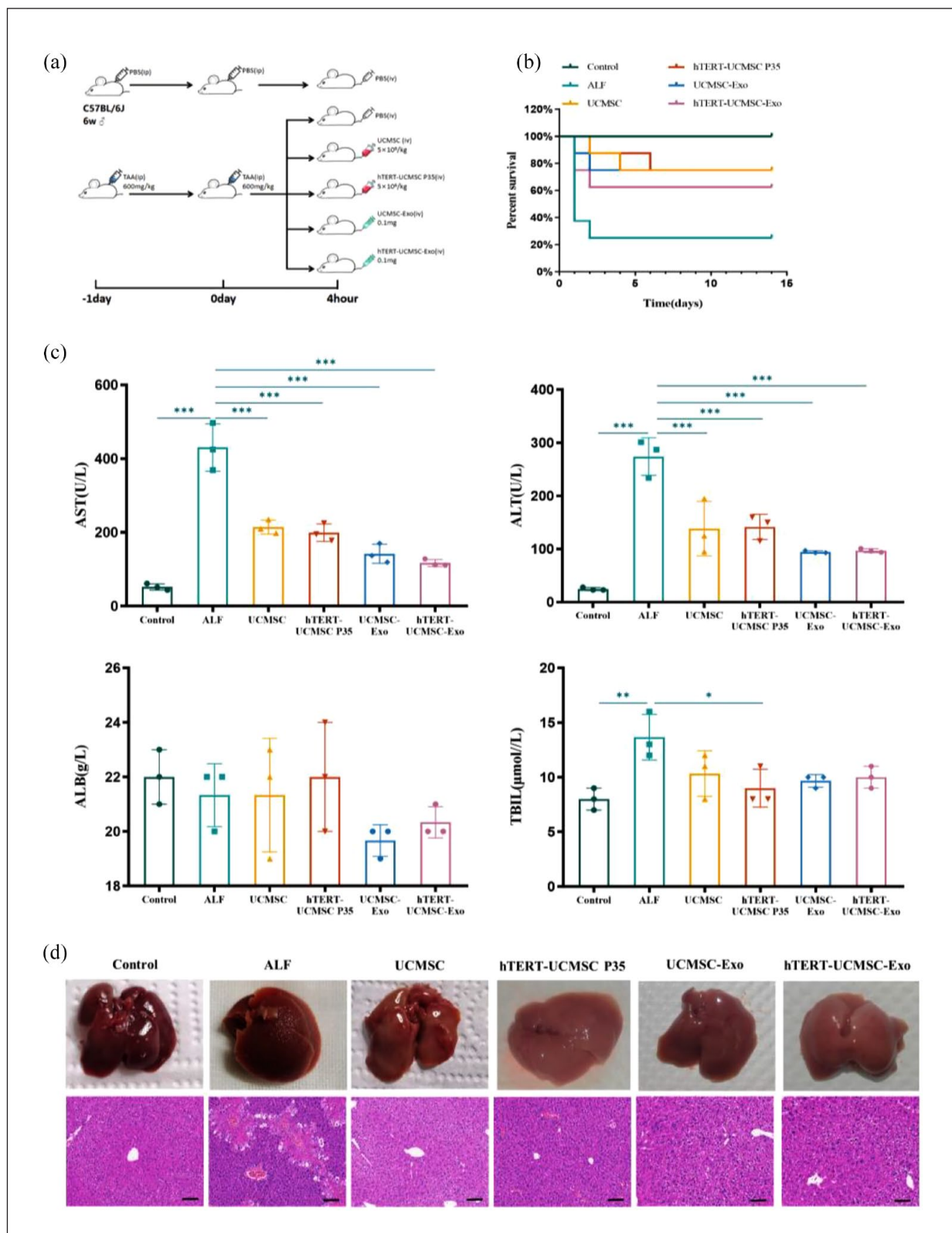
Figure 9. Therapeutic efficacy of hTERT-UCMSC and hTERT-UCMSC-Exo improved the liver functions and reduced hepatic damage in ALF mice. (a) Diagram of experimental design of cell treatment and exosomes treatment. (b) Survival curve of ALF mice treated by cell inoculation and exosomes infusion in mice. $n = 8$. (c) Examinations of liver function indexes including AST, ALT, ALB, and TBIL. $*p < 0.05$, $**p < 0.01$, $***p < 0.001$, $n = 3$. (d) Gross and HE staining images of livers from mice on day 3 after treatment. The scale bar = 100 μm.

respectively. There was no significant difference in ALB value between the two groups ($p > 0.05$). However, compared with the ALF group, AST and ALT decreased significantly in cells and exosomes treatment groups on day 3. In UCMSC treatment group, AST and ALT decreased by 50.20% ($p < 0.001$) and 49.53% ($p < 0.001$), respectively, while ALB and TBIL values showed no significant difference between the two groups ($p > 0.05$). In the hTERT-UCMSC P35 treatment group, AST, ALT and TBIL decreased by 53.68% ($p < 0.001$), 48.28% ($p < 0.001$), and 34.14% ($p < 0.05$), respectively, and there was no significant difference in ALB value between ALF group and hTERT-UCMSC P35 treatment group ($p > 0.05$). In UCMSC-Exo treatment group, AST and ALT decreased by 67.00% ($p < 0.001$) and 31.81% ($p < 0.001$), respectively, while ALB and TBIL values showed no significant difference between the two groups ($p > 0.05$). In hTERT-UCMSC-Exo treatment group, AST and ALT decreased by 72.81% ($p < 0.001$) and 29.88% ($p < 0.001$), respectively, while ALB and TBIL values showed no significant difference between the two groups ($p > 0.05$). Statistical analysis of differences between UCMSC and hTERT-UCMSC P35 treatment groups showed that there were no significant differences in ALT, AST, ALB and TBIL between groups ($p > 0.05$). Also, there were no significant difference between the UCMSC-Exo and hTERT-UCMSC-Exo treatment groups ($p > 0.05$). It was also found that exosomes were more effective than cell therapy.

Consistent with the biochemical results, liver cells in the control group were neatly arranged with clear hepatic lobule structure and no inflammatory cell infiltration under HE staining. The liver structure of mice in TAA induced ALF group was obviously damaged. Extensive necrosis and inflammatory cells infiltrated in the surrounding area of portal vein could be seen. The results of UCMSC treatment group, hTERT-UCMSC P35 treatment group, UCMSC-Exo treatment group, hTERT-UCMSC-Exo treatment group showed irregular liver tissue, irregular arrangement of liver cells and infiltration of inflammatory cells in the area around portal vein. There was no significant difference among the four treatment groups, but liver tissue was significantly repaired compared with ALF group. These results indicate that intravenous injection of either primary UCMSC, hTERT-UCMSC P35 or their exosomes can alleviate TAA-induced liver injury (Figure 9(d)).

Discussion

In this study, an immortalized cell line hTERT-UCMSC was established by stably expressing hTERT gene ectopically with lentiviral vectors in UCMSC. The results suggest that both hTERT-UCMSC (at P35) and its exosomes have similar phenotypes and characteristics to the primary UCMSC and its exosomes respectively. And this hTERT-UCMSC at

the 35th passage and its exosomes were effective in treating mice with liver failure induced by TAA.

Similar to other MSCs, the lifespan of primary UCMSCs was limited when they were cultured in vitro. Senescence usually occurs when the primary UCMSCs proliferate and divide to around 10 generations (CPDs was about 20). Large-scale production of UCMSCs and their exosomes could only be sustained by constant replenishment with new sources of MSCs from new donors. Such replenishment is not only costly because each new source must be tested and validated, but also influence the batch quality and reproducibility of MSCs and their exosome production. For the purpose of cell and exosome production, immortalized UCMSC cell lines, that are able to generate infinitely expansible clonal cell lines, are needed, which could be used as a stable cell source for manufacturing UCMSCs and their exosomes.

Replicative senescence is a common feature of all somatic cells and most stem cells. After a period of proliferation, the rate of cell division slows down and the cells are unable to divide further. This phenomenon is accompanied by some changes such as increased cell size and cell flattening, nuclear changes, and altered gene and protein expression patterns.[22,23] It is generally believed that genetic instability after severe telomere shortening leads to replicative senescence of cells.[24] Studies have proved that ectopic expression of TERT can maintain telomere length in cells, and thus immortalize cells and prevent cell function loss. Overexpression of hTERT can not only inhibit aging, but also reduce oxidative stress level by controlling mitochondria, significantly reduce the level of aneuploidy, prevent the disorder of ploidy control genes, and contribute to genetic stability.[25] We therefore overexpressed hTERT to establish the immortalized cell line hTERT-UCMSC. Our results confirmed that the immortalized UCMSC with stable hTERT overexpression increased the ability of cell proliferation. And this cell line (even at 35th passage) maintained the characteristics of MSC markers, stemness, multipotency and expression level of senescence related β -galactosidase activity similar to the early stage of primary UCMSC. Moreover, the immortalized hTERT-UCMSC also exhibits similar potential in facilitating angiogenesis and enhanced anti-stress capabilities compared to primary UCMSC. These characteristics give it additional advantage for future applications.

Although the available data indicate that lentiviral vectors are safe vectors for in vivo gene therapy.[26] The safety problem caused by the introduction of lentiviral vectors still needs investigation. Moreover, the potential tumorigenicity of hTERT-expressing stem cells remains controversial.[27] Therefore, we further verify the safety of hTERT-UCMSC. STR experiment confirmed that there was no cross contamination of hTERT-UCMSC. The results of karyotyping indicated that the immortalized hTERT-UCMSC at P10 and P35 maintained normal

karyotype even after multiple passages, which was the same as the original primary UCMSC at P3. HTERT-UCMSC showed no signs of tumorigenesis in in vitro and in vivo tumorigenic experiments. The in vivo toxicity of hTERT-UCMSC was also performed by tail vein injection of 1×10^8 cells/kg body weight. This dosage is about 100 times of generally used clinical therapeutic dosage of cell inoculation.[28] No death or abnormal signs were seen in tested mice during the 13-week observation period. These results suggest that the immortalized UCMSC in this study is safe both in vitro and in vivo.

We investigated exosomes derived from the hTERT-UCMSC. Exosomes are extracellular vesicles 50–150 nm in diameter. In this experiment, we compared the characteristics of exosomes derived from P10 and P35 hTERT-UCMSC with those derived from UCMSC. We found that exosomes from both hTERT-UCMSC P10 and P35 were similar to those derived from primary cells in morphology, phenotype, and yield. By detecting the biodistribution of exosomes in vivo, we found that exosomes-derived from hTERT-UCMSC could rapidly accumulated in the liver and spleen, which is consistent with the results of previous studies.[29] The liver is one of the major organs for the transient retention of exosomes, suggesting that this characteristic would be beneficial for liver diseases.[30]

To verify the consistency of the composition of exosomes derived from hTERT-UCMSC and UCMSC, we first conducted an analysis of several crucial miRNAs (miRNA-126-3p, miRNA-139-5p, miRNA-146a-5p, and miRNA-223-5p. Previous study has proved that miRNA-126-3p possesses angiogenesis-promoting ability.[27] The miR-139-5p and miR-146a-5p have been shown to have anti-inflammatory and antifibrotic effects on the liver.[28–30] Additionally, miR-223-5p has been reported to be associated with the anti-inflammatory properties of MSCs. Compared to exosomes derived from aging MSCs, exosomes from young MSCs exhibit higher expression levels of miR-223-5p, which is known to induce M2 polarization.[31] These effects are particularly relevant for the potential use of MSC in liver disease treatment. Our data revealed that the expression levels of these miRNAs were similar among groups of hTERT-UCMSC (P10 and P35) and UCMSC. The immunoregulatory cytokines including TGF-β, IL-10, and PD-L1 in exosomes were also detected in this study. And similarly, we did not observe any significant differences in the levels of these proteins among the various groups studied. These findings suggest that in exosomes from hTERT-UCMSC, the levels of crucial factors associated with therapeutic effects of MSC are comparable to those in primary MSC-derived exosomes.

Studies have shown that both inoculation of MSCs[31–37] and MSCs-derived exosomes[20,38,39] can improve liver function, inhibit hepatocyte apoptosis and promote hepatocyte proliferation in ALF animal models. However, whether the immortalized UCMSC after long-term passage and its exosomes can be effective in treating ALF remains unknown. We evaluated the effect of the immortalized UCMSC and its exosomes in rescuing ALF mice induced by TAA. Our study found that compared with the control group, both primary UCMSC (P3~P6) and hTERT-UCMSC (P35) could significantly relieve liver injury, improve liver function and increase the survival rate of mice with ALF from 25% to 75%. Similarly, injection of both primary MSC and immortalized cell-derived exosomes (P35) displayed a good therapeutic effect on mice with liver failure. Although the survival rate in hTERT-UCMSC P35 Exo group (62.5%) is slightly lower that of UCMSC-Exo group (75%), there was no significant difference in the survival rates between these two groups. These results indicate that both immortalized hTERT-UCMSC and its exosomes have promising clinical value in the treatment of ALF. Immortalized hTERT-UCMSC is expected to become an ideal "seed cell" to provide stable MSC source and MSC-derived exosomes for ALF therapy.

The mechanisms of hTERT-UCMSC improving liver function and survival rate of ALF mice have not been clarified. Previous studies suggest that the mechanisms underlying the MSC therapy mainly includes the following two aspects: ① First, MSC immune regulation alleviates the inflammation in TAA-induced ALF mice. MSC convey regulatory signals to recipient immune cells in the microenvironment by releasing a wide variety of cytokines, chemokines, exosomes, and trophic factors.[6,40] Among them, TGF-β and IL-10 are considered to be the key factors that support immune homeostasis.[41] Similarly, PD-L1 may be involved in immune regulation stimulated by MSCs.[42] In addition, MSC is able to regulate adaptive and innate immune responses by inhibiting T and dendritic cells, reducing B cell activation and proliferation, promoting regulatory T cell production, and inhibiting natural killer cell proliferation and cytotoxicity.[43–48] In the preliminary validation of hTERT-UCMSC, it was found that the secretion of inflammatory regulatory cytokines was similar to that of primary cell, and was not affected by the cell generation. This also suggests that hTERT-UCMSC may play a therapeutic role through immunomodulatory properties. ② MSC might differentiate into hepatocyte like cell (HLC). Some studies have suggested that UCMSC inoculation can significantly improve the survival rate of ALF rats induced by carbon tetrachloride, and the potential mechanism may involve the transformation of UCMSC into HLC and its directed migration to the site of liver injury.[31,49] However, some other studies pointed out that MSC cannot directly differentiate into HLC in vivo.[50,51] Our study also found that after cell transplantation, the cells only remained in the liver tissue for a short period of time and were essentially eliminated after 5 days. Therefore, this mechanism does not hold true in our study.

Our study also indicated that exosomes from hTERT-UCMSC (P35) have similar therapeutic effects on mice with ALF. The mechanisms of exosomes from UCMSCs on ALF are still not clear. It has been reported that a variety of bioactive compounds, including proteins, mRNA, DNA, miRNA, and lipids, enable exosomes to play roles in immune regulation and cell communication.[52] In addition, some studies have shown that non-coding RNAs enriched in exosomes are the main effector of exosome-mediated liver protection.[53] However, in this study, we only detected the levels of several miRNAs and immunoregulatory proteins in exosomes from hTERT-UCMSC which are known to play a role in the therapeutic effects of MSCs. More studies are needed to investigate the mechanisms involved in the effects of UCMSC on ALF.

There are limitations in our study. Firstly, the safety and efficacy uncertainty still exist as we only examined the in vitro and in vivo safety and efficacy using the hTERT-UCMSC at passage 35. The test using higher generation of hTERT-UCMSC should be carried out. Secondly, this study was limited by the lack of data from large animal studies, such as pigs and primates.

Conclusion

In this study, we successfully constructed an immortalized cell line from UCMSC, the hTERT-UCMSC. The hTERT-UCMSC and its exosomes maintain the main characteristics even after long-term passage. And inoculation of hTERT-UCMSC and hTERT-UCMSC-Exo were safe and effective in treating mice with ALF. This immortalized cell line could be a promising "seed cell" for MSC and its exosome-based therapy for liver failure.

Declaration of conflicting interests

The author(s) declared no potential conflicts of interest with respect to the research, authorship, and/or publication of this article.

Ethical approval

The study protocols were reviewed and approved by the Zhujiang Hospital review board and ethics committee of Zhujiang Hospital of Southern Medical University. All experiments involving mice have been reviewed and approved by the Animal Ethics Committee of Southern Medical University Zhujiang Hospital.

ORCID iDs

Lei Feng (iD) https://orcid.org/0000-0001-6053-8417
Yi Gao (iD) https://orcid.org/0000-0002-4536-6191
Shuqin Zhou (iD) https://orcid.org/0000-0002-4301-7780
Qing Peng (iD) https://orcid.org/0000-0002-7790-6455

Supplemental material

Supplemental material for this article is available online.

References

1. Liu QW, Liu QY, Li JY, et al. Therapeutic efficiency of human amniotic epithelial stem cell-derived functional hepatocyte-like cells in mice with acute hepatic failure. *Stem Cell Res Ther* 2018; 9(1): 321.
2. Bernal W, Lee WM, Wendon J, et al. Acute liver failure: a curable disease by 2024? *J Hepatol* 2015; 62(1 Suppl): S112–S120.
3. Stravitz RT and Lee WM. Acute liver failure. *Lancet* 2019; 394(10201): 869–881.
4. Zhou W, Nelson ED, Abu Rmilah AA, et al. Stem cell-related studies and stem cell-based therapies in liver diseases. *Cell Transplant* 2019; 28(9-10): 1116–1122.
5. Lin H, Xu R, Zhang Z, et al. Implications of the immunoregulatory functions of mesenchymal stem cells in the treatment of human liver diseases. *Cell Mol Immunol* 2011; 8(1): 19–22.
6. Wang YH, Wu DB, Chen B, et al. Progress in mesenchymal stem cell-based therapy for acute liver failure. *Stem Cell Res Ther* 2018; 9(1): 227.
7. Guo G, Zhuang X, Xu Q, et al. Peripheral infusion of human umbilical cord mesenchymal stem cells rescues acute liver failure lethality in monkeys. *Stem Cell Res Ther* 2019; 10(1): 84.
8. Hu C, Wu Z and Li L. Mesenchymal stromal cells promote liver regeneration through regulation of immune cells. *Int J Biol Sci* 2020; 16(5): 893–903.
9. Wu L, Tian X, Zuo H, et al. miR-124-3p delivered by exosomes from heme oxygenase-1 modified bone marrow mesenchymal stem cells inhibits ferroptosis to attenuate ischemia-reperfusion injury in steatotic grafts. *Nanobiotechnol* 2022; 20(1): 196.
10. Roefs MT, Sluijter JPG and Vader P. Extracellular vesicle-associated proteins in tissue repair. *Trends Cell Biol* 2020; 30(12): 990–1013.
11. Kalluri R and LeBleu VS. The biology, function, and biomedical applications of exosomes. *Science* 2020; 367(6478): eaau6977.
12. Shu S, Yang Y, Allen CL, et al. Purity and yield of melanoma exosomes are dependent on isolation method. *J Extracell Vesicles* 2020; 9(1): 1692401.
13. Wang Y, Pei YA, Sun Y, et al. Stem cells immortalized by hTERT perform differently from those immortalized by SV40LT in proliferation, differentiation, and reconstruction of matrix microenvironment. *Acta Biomater* 2021; 136: 184–198.

14. Zhang Y, Li Y, Li W, et al. Therapeutic effect of human umbilical cord mesenchymal stem cells at various passages on acute liver failure in rats. *Stem Cells Int* 2018; 2018: 7159465.

15. Zhang Y, Shi J and Liu S. Establishment and characterization of a telomerase-immortalized sheep trophoblast cell line. *Biomed Res Int* 2016; 2016: 1–9.

16. Zhang H, Huang Y, Wang L, et al. Immortalization of porcine placental trophoblast cells through reconstitution of telomerase activity. *Theriogenology* 2016; 85(8): 1446–1456.

17. Trachana V, Petrakis S, Fotiadis Z, et al. Human mesenchymal stem cells with enhanced telomerase activity acquire resistance against oxidative stress-induced genomic damage. *Cytotherapy* 2017; 19(7): 808–820.

18. Zhang Y, Liu J, Mo Y, et al. Immortalized mesenchymal stem cells: a safe cell source for cellular or cell membrane-based treatment of glioma. *Stem Cells Int* 2022; 2022: 6430515–6430565.

19. Tsai CC, Chen CL, Liu HC, et al. Overexpression of hTERT increases stem-like properties and decreases spontaneous differentiation in human mesenchymal stem cell lines. *J Biomed Sci* 2010; 17(1): 64.

20. Shokravi S, Borisov V, Zaman BA, et al. Mesenchymal stromal cells (MSCs) and their exosome in acute liver failure (ALF): a comprehensive review. *Stem Cell Res Ther* 2022; 13(1): 192.

21. Wang H, Wang T, Rui W, et al. Extracellular vesicles enclosed-miR-421 suppresses air pollution (PM$_{2.5}$)-induced cardiac dysfunction via ACE2 signalling. *J Extracell Vesicles* 2022; 11(5): e12222.

22. Campisi J. The biology of replicative senescence. *Eur J Cancer* 1997; 33(5): 703–709.

23. Cristofalo VJ, Lorenzini A, Allen RG, et al. Replicative senescence: a critical review. *Mech Ageing Dev* 2004; 125(10–11): 827–848.

24. Herbig U, Jobling WA, Chen BP, et al. Telomere shortening triggers senescence of human cells through a pathway involving ATM, p53, and p21(CIP1), but not p16(INK4a). *Mol Cell* 2004; 14(4): 501–513.

25. Estrada JC, Torres Y, Benguría A, et al. Human mesenchymal stem cell-replicative senescence and oxidative stress are closely linked to aneuploidy. *Cell Death Dis* 2013; 4(6): e691.

26. Levine BL, Humeau LM, Boyer J, et al. Gene transfer in humans using a conditionally replicating lentiviral vector. *Proc Natl Acad Sci USA* 2006; 103(46): 17372–17377.

27. Kelland LR. Overcoming the immortality of tumour cells by telomere and telomerase based cancer therapeutics – current status and future prospects. *Eur J Cancer* 2005; 41(7): 971–979.

28. He J, Ruan GP, Yao X, et al. Chronic toxicity test in cynomolgus monkeys for 98 days with repeated intravenous infusion of cynomolgus umbilical cord mesenchymal stem cells. *Cell Physiol Biochem* 2017; 43(3): 891–904.

29. Yeo RW, Lai RC, Zhang B, et al. Mesenchymal stem cell: an efficient mass producer of exosomes for drug delivery. *Adv Drug Deliv Rev* 2013; 65(3): 336–341.

30. Yi YW, Lee JH, Kim SY, et al. Advances in analysis of biodistribution of exosomes by molecular imaging. *Int J Mol Sci* 2020; 21(2): 665.

31. Zheng S, Yang J, Yang J, et al. Transplantation of umbilical cord mesenchymal stem cells via different routes in rats with acute liver failure. *Int J Clin Exp Pathol* 2015; 8(12): 15854–15862.

32. Huang B, Cheng X, Wang H, et al. Mesenchymal stem cells and their secreted molecules predominantly ameliorate fulminant hepatic failure and chronic liver fibrosis in mice respectively. *J Transl Med* 2016; 14: 45.

33. Gilsanz C, Aller MA, Fuentes-Julian S, et al. Adipose-derived mesenchymal stem cells slow disease progression of acute-on-chronic liver failure. *Biomed Pharmacother* 2017; 91: 776–787.

34. Tautenhahn HM, Brückner S, Baumann S, et al. Attenuation of postoperative acute liver failure by mesenchymal stem cell treatment due to metabolic implications. *Ann Surg* 2016; 263(3): 546–556.

35. Cai Y, Zou Z, Liu L, et al. Bone marrow-derived mesenchymal stem cells inhibits hepatocyte apoptosis after acute liver injury. *Int J Clin Exp Pathol* 2015; 8(1): 107–116.

36. Zhu M, Hua T, Ouyang T, et al. Applications of mesenchymal stem cells in liver fibrosis: novel strategies, mechanisms, and clinical practice. *Stem Cells Int* 2021; 2021: 65467801–65467817.

37. Kolodziejczyk AA, Federici S, Zmora N, et al. Acute liver failure is regulated by myc- and microbiome-dependent programs. *Nat Med* 2020; 26(12): 1899–1911.

38. Shao M, Xu Q, Wu Z, et al. Exosomes derived from human umbilical cord mesenchymal stem cells ameliorate IL-6-induced acute liver injury through miR-455-3p. *Stem Cell Res Ther* 2020; 11(1): 37.

39. Kostallari E, Valainathan S, Biquard L, et al. Role of extracellular vesicles in liver diseases and their therapeutic potential. *Adv Drug Deliv Rev* 2021; 175: 113816.

40. Markov A, Thangavelu L, Aravindhan S, et al. Mesenchymal stem/stromal cells as a valuable source for the treatment of immune-mediated disorders. *Stem Cell Res Ther* 2021; 12(1): 192.

41. Vignali DA, Collison LW and Workman CJ. How regulatory T cells work. *Nat Rev Immunol* 2008; 8(7): 523–532.

42. Gu YZ, Xue Q, Chen YJ, et al. Different roles of PD-L1 and FasL in immunomodulation mediated by human placenta-derived mesenchymal stem cells. *Hum Immunol* 2013; 74(3): 267–276.

43. Akiyama K, Chen C, Wang D, et al. Mesenchymal-stem-cell-induced immunoregulation involves FAS-ligand-/FAS-mediated T cell apoptosis. *Cell Stem Cell* 2012; 10(5): 544–555.

44. Fang X, Liu L, Dong J, et al. A study about immunomodulatory effect and efficacy and prognosis of human umbilical cord mesenchymal stem cells in patients with chronic hepatitis B-induced decompensated liver cirrhosis. *J Gastroenterol Hepatol* 2018; 33(4): 774–780.

45. Zhang Y, Cai W, Huang Q, et al. Mesenchymal stem cells alleviate bacteria-induced liver injury in mice by inducing regulatory dendritic cells. *Hepatology* 2014; 59(2): 671–682.

46. Corcione A, Benvenuto F, Ferretti E, et al. Human mesenchymal stem cells modulate B-cell functions. *Blood* 2006; 107(1): 367–372.

47. Milosavljevic N, Gazdic M, Simovic Markovic B, et al. Mesenchymal stem cells attenuate acute liver injury by

altering ratio between interleukin 17 producing and regulatory natural killer T cells. *Liver Transpl* 2017; 23(8): 1040–1050.

48. Zhu X, He B, Zhou X, et al. Effects of transplanted bone-marrow-derived mesenchymal stem cells in animal models of acute hepatitis. *Cell Tissue Res* 2013; 351(3): 477–486.

49. Shi LL, Liu FP and Wang DW. Transplantation of human umbilical cord blood mesenchymal stem cells improves survival rates in a rat model of acute hepatic necrosis. *Am J Med Sci* 2011; 342(3): 212–217.

50. Xiao JQ, Shi XL, Ma HC, et al. Administration of IL-1Ra chitosan nanoparticles enhances the therapeutic efficacy of mesenchymal stem cell transplantation in acute liver failure. *Arch Med Res* 2013; 44(5): 370–379.

51. Chen G, Jin Y, Shi X, et al. Adipose-derived stem cell-based treatment for acute liver failure. *Stem Cell Res Ther* 2015; 6: 40.

52. Doyle L and Wang M. Overview of extracellular vesicles, their origin, composition, purpose, and methods for exosome isolation and analysis. *Cells* 2019; 8(7): 727.

53. Wang C, Zhou H, Wu R, et al. Mesenchymal stem cell-derived exosomes and non-coding RNAs: regulatory and therapeutic role in liver diseases. *Biomed Pharmacother* 2023; 157: 114040.